Ballistic emission microscopy studies on metal–molecule interfaces



2008 J. Phys.: Condens. Matter 20 374113

(http://iopscience.iop.org/0953-8984/20/37/374113)

IOP PUBLISHING JOURNAL OF PHYSICS: CONDENSED MATTER

J. Phys.: Condens. Matter **20** (2008) 374113 (10pp) doi:10.1088/0953-8984/20/37/374113

# Ballistic emission microscopy studies on metal–molecule interfaces

**N Chandrasekhar**

Institute of Materials Research and Engineering, 3 Research Link, 117602, Singapore

Received 15 February 2008, in final form 25 March 2008
Published 26 August 2008
Online at stacks.iop.org/JPhysCM/20/374113

**Abstract**

Ballistic electron emission microscopy (BEEM) experiments on metal–molecule interfaces are briefly reviewed. Results of BEEM experiments with two different orientations of molecules are presented and discussed. Significant differences in uniformity of transport through the molecular layer are found. Implications for device applications are briefly discussed.

(Some figures in this article are in colour only in the electronic version)

## 1. Introduction

The field of molecular electronics was born over 35 years ago, with the concept of a molecular rectifier given by Aviram and Ratner [1]. Molecular electronics is a growing area of theoretical and experimental research (see [2] and references therein). Even the simplest future application, such as a molecular memory, will require molecular rectifiers which meet very stringent performance criteria. Some of these criteria are large current rectification, small time constants, large breakdown voltages, and sharp voltage thresholds. The primary problems faced by the molecular electronics community are measuring and calculating charge transport through molecules. Molecular electronics also demands reliable molecular wires to carry signals from one circuit element to another.

The ability to measure conductivity of a single molecule is a necessary requirement in all of the above experiments. This requires the connection of a macroscopic current source and voltmeter to each end of a molecule. The connections should exhibit ohmic behavior with a low contact resistance, so that measured electrical characteristics can be unambiguously attributed to the molecule. By now, sufficient evidence exists to indicate that simply making physical contact between a metal and molecule is not enough to guarantee good electrical contact. The problem is compounded by the fact that the interfaces are buried under a thin film of metal. Therefore, the problem is one of contacts—how to make them, and how to characterize them at length scales that are relevant for molecular electronics applications.

Metal–molecule contacts or interfaces have traditionally been investigated by current–voltage ($I$–$V$), capacitance–voltage ($C$–$V$) and ultraviolet (UV) spectroscopy, all of which average over micrometer scale or larger areas [3–7]. In contrast, prototype devices incorporating molecules as active components are in the nm range [2]. Organic device configurations that have been investigated to date are either self-assembled monolayers (SAM) [2] and references therein or Langmuir–Blodgett (LB) films [6]. At the present time, it is unclear whether the inhomogeneities in electrical behavior originate from microstructural perturbations such as asperities at the interfaces with the contacting electrodes, or whether they are an inherent electronic property of metal–molecule interfaces. SAM and LB films are not rigid, and despite the implementation of precautionary measures, it is uncertain whether the integrity of the organic is maintained after deposition of the metal film [8]. For instance, in metal–inorganic semiconductor (MIS) interfaces, unless the semiconductor surface is prepared with care and the metal is chosen so that it is lattice matched, the metal film is polycrystalline, causing significant variations in the electronic transparency of the interface [9, 10].

Several different techniques have been developed to contact molecules, such as use of Hg drops [11], metalization by physical vapor deposition [12, 13], use of Au nanoparticles to contact functionalized molecules in an inert matrix [14]. Break junctions [15], and pores etched in Si wafers have also been used [16]. All of these techniques have the advantage of nanometer scale spatial resolution; however, they yield $I$–$V$ s on the metal–molecule–metal assembly. None of them probes the metal–molecule interface itself.

Some of the work on metal–molecule interfaces is briefly, and for reasons of brevity, incompletely and inadequately summarized below. Ho and colleagues [16] have reported the most comprehensive and systematic experimental work on metal atom–single molecule interactions, by STM spectroscopy, and images of a metal–molecule–metal bridge. They report a splitting and shifting of molecular orbitals and

 

formation of an extended molecule. There is a modification of the local density of states (LDOS) of the electrode, due to hybridization of the electron wavefunctions of the metal with the electron wavefunctions of the molecule. These factors determine the alignment of molecular orbital energies with the metal Fermi level, as well as the strength of the coupling. In macroscale experiments, Zhitenev *et al* [17] find no doping of the molecular layer due to the contact with a metal electrode.

Datta *et al* [18] report a drop in electrostatic potential at the metal–molecule interface from STM studies on self-assembled monolayers. Vuillaume *et al* [19] report a higher conductivity in disordered monolayers. They also find a reduced tunneling contribution to the overall conductivity of the SAM, when the organic is densely packed and highly ordered. Williams *et al* [20] show that rectification by metal–molecule–metal structures arises due to asymmetric coupling of a molecular level to the metal electrodes through tunnel barriers, and is independent of the work function difference. Temirov *et al* [21] have reported free electron like dispersion in an organic monolayer film consisting of perylenetetracarboxylic-acid-dianhydride (PTCDA) molecules on an Ag(111) surface.

In a series of papers, Xue and Ratner [22, 23] have presented the most comprehensive treatment of charge transport through metal–molecule interfaces. They have shown that the local structure of the metal, at the metal–molecule interface, has an effect on transport through the molecule. The have also shown that, depending on the molecule, the voltage drop can be at the metal–molecule interface, or there can be a voltage drop in the molecular core as well. They also show that the local electrochemical potential can vary over distances as small as 1 Å, which is of the order of the Fermi wavelength of electrons in the metal. This observation stresses the importance of atomic scale analysis for studying effects in single-molecule electronics, such as in the experiments by Ho *et al* [16] or other kinds of experiments. There are subtle differences of the geometries of the metal–molecule structures investigated by Ho [16] and Ratner [22, 23]. The phenyl molecules studied by Ratner [22, 23] are thiolated, and bind to an Au substrate so that the molecules stand upright. In contrast the phthalocyanine molecules investigated by Ho lie down flat on a thin layer of insulator grown by oxidation on a metal surface. Clearly, there is a need for an experiment that can access both geometries, and study metal–molecule contacts that can be fabricated in a reproducible manner, with ångström or nanometer scale resolution. There is also a large body of experimental work on single-molecule electronic properties, such as imaging of the HOMO and LUMO, the effect of metal atoms in close proximity to the molecule, switching effects in single molecules etc, which have not been mentioned above, since the focus of this article is metal–molecule interfaces.

BEEM, a variant of STM, has been used to study metal–organic interfaces and metal–SAM structures with nanometer scale lateral resolution [24, 25]. The groups of Hsu *et al* [24] and Oezcan *et al* [25] have reported results on metal–self-assembled monolayer–inorganic semiconductor interfaces. There is evidence that the chemisorption of alkanethiol monolayers on inorganic semiconductors increases the metal–inorganic semiconductor Schottky barrier when the inorganic

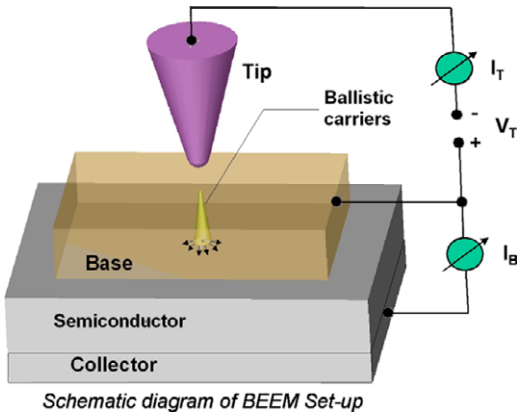


**Figure 1.** Schematic of a ballistic emission microscopy experiment. The buried metal–semiconductor interface is studied.

semiconductor is GaAs. The Schottky barrier remains the same when the inorganic semiconductor is Si. Bannani *et al* [26] have demonstrated ballistic electron microscopy of individual molecules of the fullerene $C_{60}$, and PTCDA on Bi(111) overlayers, grown on Si(100) substrates. They found characteristic submolecular patterns that indicated attenuation or enhancement of ballistic transport. Their technique has been called 'scanning near field electron transmission microscopy'. Kirczenow [27] has pointed out that the propagation of ballistic carriers through molecular layers will be so strongly attenuated that it is possible only to observe resonant tunneling.

In this paper, we use ballistic electron emission spectroscopy and microscopy to study charge transport across Ag–terthiophene (T3C$x$SH) ($x = 4, 8$)-on-Au interfaces, and Pt–trizigzag-HBC–Ph$x$ ($x = 3, 6$)–Pt interfaces. The objective is to understand the effect of molecular orientation on charge transport through the metal–molecule interface. The terthiophene molecules stand upright, while the HBC molecules lie down flat on the metal substrates. The latter has a structure analogous to that of graphene. The BEEM technique allows us to image charge transport across the metal–molecule interfaces with nanometer scale spatial resolution, unlike conventional spectroscopy and current–voltage measurements that average over millimeter areas.

A schematic of BEEM is shown in figure 1. A semiconductor (polymer/oligomer or self-assembled monolayer) is overlaid with a thin metal film (thickness $< 10$ nm, termed the base), with an ohmic contact underneath, termed the collector. The top metal film (base) is grounded, and carriers are injected into it using a scanning tunneling microscope (STM) tip. At energies sufficiently higher than the metal's Fermi energy, these carriers propagate in a ballistic manner (without any scattering) in the base, prior to incidence on the interface. There is spreading of carriers in the metal film due to mutual Coulomb repulsion and interaction with the Fermi sea. These interactions determine the lateral resolution of the BEEM technique. If the energy of the carriers exceeds the local band offset or Schottky/injection barrier, they propagate into the organic/molecule and can be collected from the contact at the bottom. Typically the tunneling current is attenuated by a factor of 1000, so collector currents are in the picoampere range.

Both spectroscopy and imaging can be done on this structure, by monitoring the collector current as a function of STM tip bias voltage at a fixed location, or as a function of tip position at a fixed STM tip bias. One of the fundamental advantages of BEEM is the ability to investigate transport properties of hot electrons with high lateral resolution, typically at the nanometer scale.

## 2. Upright molecules

### *2.1. Experimental procedure*

Self-assembled monolayers of the thiolated terthiophenes with alkyl segments of different chain lengths (T3CxSH) were prepared from 1 mM in ethanol solution, and were immobilized on template-stripped gold surfaces prepared based on the procedure of Wagner *et al* [28]. The alkane segment binds to the substrate via Au–S bonds, and the terthiophene is available for the electrical contact by a metal. This allows the energy levels of the molecular orbitals of the T3 part of the SAMs to be probed by BEEM.

The silver contacts were formed by direct evaporation of Ag through a mechanical mask (1 $mm^2$ area). The film was deposited at a rate of 0.1 Å $s^{-1}$ and had a thickness of 8 nm. The chamber pressure immediately prior to evaporation was $10^{-8}$ Torr. The BEEM experiments were done at 77 K in a home-assembled STM system. We wish to point out that the yield of BEEM diodes is quite low, typically <5%. This is a problem which currently hampers routine BEEM experiments with organic SAMs. The current noise of the set-up is typically 1 pA. Conventional $I$–$V$ measurements were carried out on a different set of samples, prepared from the same solution as the BEEM samples, in a standard semiconductor probe station to verify diode behavior and to monitor diode stability. In probe station experiments, indium (In) was used instead of silver (Ag) as the top electrode after SAM formation, for ease of preparation, since the work function of In is relatively close to that of Ag. It should be noted that Schottky $I$–$V$ curves are sensitive to pressure. Therefore, an indium dot (≈0.5 mm in diameter) was brought into contact with minimal pressure so as to avoid applying stress, and potential damage to the molecules or the interface. The $j$–$V$ curves obtained from these measurements will be discussed after the BEEM results are presented.

First-principles density functional theory was used to calculate the structure and orbital energy levels of T3C4SH and T3C8SH molecules. The electronic structure calculations were performed using the B3LYP functional as implemented in the Gaussian 03 [29] package. Geometry optimization was done using the 6-31G(d, p) polarized double-zeta basis set and orbital energies were obtained using the larger 6-311G(d, p) polarized triple-zeta basis. The accuracy of this level of theory has been confirmed for pi-conjugated systems [30] as well as for oligothiophenes [31, 32].

In the optimized structure the three thiophene molecules of T3C4SH and T3C8SH are non-planar with dihedral angles of 10° between the left and middle rings, and 17° between the middle and right rings, in agreement with Zhou *et al* [33]. Since the torsional angles between the thiophene rings might significantly affect the orbital energy levels, we also calculated the orbital energies for the symmetrical planar structure. The planar structure was found to be 0.7 kJ $mol^{-1}$ higher than the non-planar structure, indicating thiophene torsion to be fairly easy to achieve. The orbital energies for the highest occupied molecular orbital (HOMO) and for the lowest unoccupied molecular orbital (LUMO) were calculated for both molecules using the above procedure. As can be expected from the improved orbital overlap, the HOMO energy level is slightly higher in the planar structure, whereas the LUMO energy level is slightly lower. However, the effect on the energy gap is rather small at 0.07 eV. The molecular orbitals are almost entirely located on the thiophene part of the molecule. To validate the accuracy of our theoretical predictions, we also calculated the HOMO–LUMO gap for terthiophene (3T). Our calculated value of 3.42 eV is in reasonable agreement with an experimental value of 3.1 eV [34] and with a theoretical value of 3.5 eV reported by Beljonne *et al* [35]. The HOMO–LUMO gap for the T3 molecule is very similar to the energy gap for the T3C4SH and T3C8SH molecules, consistent with these results.

BEEM spectra and images of the buried interface are collected, by monitoring the collector current as a function of tip bias voltage or lateral position. Ballistic hole emission spectra (BHES) are obtained by recording the current at the Au collector as a function of positive voltage applied between the tip and the Ag base. Typically, several tens of individual $I$–$V$ curves acquired over different locations within a nominally 25 $nm^2$, are averaged in order to improve the signal to noise ratio. Repeated acquisition of spectra at the same point was found to be detrimental to the sample, as evidenced by the increased instability of the spectrum with time. The Schottky or injection barrier can be deduced from these individual or averaged curves, and is usually taken to be the point where the collector current begins to deviate from zero. Thermal broadening can cause significant deviations of the measured barrier from BEEM spectra. However, thermal effects are negligible for BEEM spectra acquired at 77 K, for the barriers measured in this work.

Images of the barrier transparency are obtained at specific voltages, usually above the Schottky barrier value, by scanning an area with the STM tip and recording the current at the collector. It is important to ensure that the Ag film is reasonably flat, since the base is held at ground potential. Unless this requirement is met, attempts to tunnel into patches of the metal film which are poorly connected can lead to tip crashes. Furthermore, if lateral variations of the Fermi level of the Ag occur due to poor connectivity, incorrect values of the Schottky/injection barrier will be obtained [9, 10].

We now present the BEEM results for the SAMs with the following convention. The first panel will show the STM topography, the second panel will show the BEEM current image, the third panel will show the BEEM spectrum, and the last panel will show the STM $z$–$V$ spectroscopy results. Additionally, the STM distance versus potential spectra are taken at room temperature under atmospheric pressure using a platinum iridium tip on the T3C$x$SH/Au sample. In this STM-based technique, the $z$–$V$ curve probes the density of

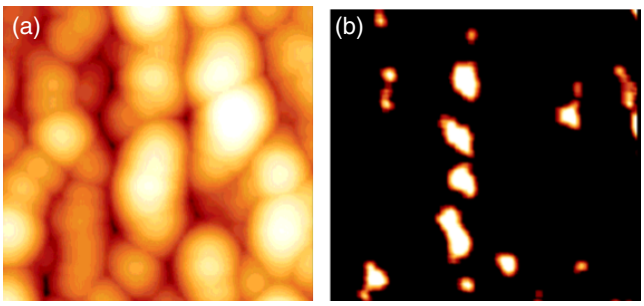


**Figure 2a.** BEEM results for the T3C4SH molecule over a 50 nm scan area. (a) STM topography of the 10 nm thick Ag film deposited on top of the SAM. (b) Corresponding BEEM image. The full scale is 8 pA.

states via the voltage dependent tip displacement at constant tunneling current [36]. By reducing the voltage, the tip is brought into close proximity and finally direct physical contact with the molecules. At a characteristic threshold bias voltage, the conduction mechanism for the carriers favors direct tunneling to the gold substrate rather than through the T3C4SH molecules. This transition is observed through a significant change of the slope in the $z$–$V$ curve.

All STM and BEEM scans will be 50 nm$^2$. This size is large enough to average over several different grains of the base (top metal film), so that features visible at this scale are attributable to the properties of the metal–molecule interface. We first show the results for the T3C4SH molecules in figure 2a. The scan area and topography full scale on this image are approximately 50 nm and 3 nm respectively and correspond to the 10 nm thick Ag film. An STM image of the top Ag film, at 0.5 V and 1 nA, is shown in figure 2a(a). The topography scale is 1.5 nm. The Ag film is well connected, and lateral variations of the Fermi level are unlikely. The grain size of the Ag film cannot be determined unambiguously.

The BEEM $I$–$V$ curve and its derivative enable a choice of imaging conditions suitable to the particular interface. For instance, based on the spectroscopy data, it is possible to determine that a bias voltage larger than 0.6 V should yield measurable collector currents. Figure 2a(b) shows a BEEM current image. The bias on the STM tip is 1 V and the tunneling current is 1 nA. The full scale current on the BEEM image is 10 pA. We find insignificant correlations between the BEEM current images and the STM image or its derivative (not shown), a fact readily apparent from the images. The scale to the right of this image indicates the range of BEEM current. The BEEM current image indicates a non-uniform transparency of the interface with bright spots that range in size from a few nanometers to about 20 nm. BEEM current directly measures the conductance of the interface as it quantifies the number of carriers being collected at the bottom electrode, at a fixed voltage that is applied to the STM tip. Averaged BEEM spectroscopy recordings of the interface taken at the bright and dark regions of the BEEM image respectively, are shown in figure 2b(c). Several tens of individual spectra, acquired over different locations within a nominally 20 nm$^2$ area, are averaged to improve the signal to noise ratio.

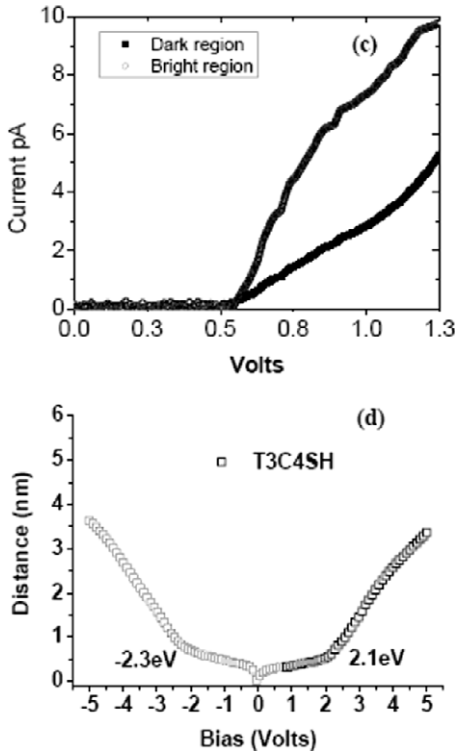


**Figure 2b.** BEEM and $z$–$V$ spectroscopy results for the T3C4SH molecule. (c) BEEM spectroscopy ($I$–$V$). (d) STM $Z$–$V$ spectroscopy showing the HOMO and LUMO levels relative to the Au Fermi level.

Extraction of the Schottky barrier height from the BEEM data can be done using the Bell and Kaiser [37] (BK) model, in which a planar tunneling formalism is used to determine its shape. The Ludeke and Prietsch [38] model uses transverse momentum ($k$ vector) conservation, and is clearly inapplicable at the MO interface, since $k$ is not a good quantum number. Both models fit experimental data for MIS interfaces, with the differences being comparable to experimental error, but are valid only in a small region of energy close to the injection barrier threshold. The functional dependence of the BEEM current on voltage is a power law $(V - V_0)^n$, where $V_0$ is the injection barrier, and the exponent $n$ ranges from 2 to 5/2. The best fit to our data is obtained with an exponent of 5/2 and a $V_0$ of 0.5 V for the two molecules—T3C4SH and T3C8SH. For both molecules, injection is from the Ag to the terthiophene segment. Therefore the same injection barrier is obtained for both molecules. The BK model has been used successfully for semiconductors with parabolic energy bands, and fits the Au–Si(100) data very well using a power law behavior in a small region near the threshold [9, 10]. The assumption of transverse wavevector conservation is justifiable for epitaxial interfaces such as $CoSi_2$/Si and $NiSi_2$/Si [9, 10]. For MO interfaces, since no matching lattice net exists, a completely different theoretical approach to analyzing BEEM data is probably required.

The BEEM spectra over the bright regions as well as the dark regions indicate a Schottky barrier of 0.5 V. We note that this is the injection barrier for holes, since the sign of the bias on the STM tip is positive. Considering the fact that the

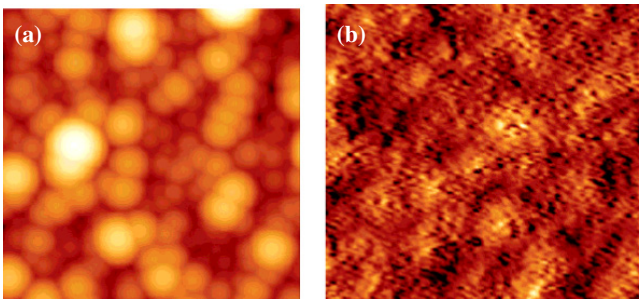


**Figure 3a.** BEEM results for the T3C4SH molecule over a 50 nm scan area. (a) STM topography of the 10 nm thick Ag film deposited on top of the SAM. (b) Corresponding BEEM image. The full scale is 10 pA.

oxidation potential for this molecule is 0.5 V, when measured relative to Ag [39], the agreement is indeed satisfactory. These results demonstrate the utility of the BEEM technique: no other technique is capable of giving a pictorial representation of charge transport across the metal–molecule interface with nanometer scale resolution.

Figure 2b(d) shows the $z$–$V$ spectrum of T3C4SH on Au. For this measurement, the bias voltage is ramped with decreasing magnitude for each polarity. The thin lines show the linear interpolation from the two distinct slopes of the averaged spectrum (shown by thick line). The intersection of these lines determines the values of electron and hole threshold voltages.

Corresponding BEEM results for T3C8SH are presented in figure 3a. First of all, there is hardly any difference in the topography of the top Ag film, as seen from figures 3a(a) and 2a(a). However, there is a dramatic difference in the BEEM current images for these two molecules, readily apparent from a comparison of figures 3a(b) and 2a(b). Finally, an injection barrier of 0.5 V is obtained for this molecule as well, as is evident from figure 3b(c). This is to be expected, since the molecular orbitals are almost entirely on the terthiophene segment. Since the Ag base physically contacts only the terthiophene segment, it is reasonable to expect that the injection barrier remains invariant with alkane segment length. Clearly, the BEEM current images for T3C8SH indicate more uniform charge transport across the interface, across the scanned area. This is to be expected, since the length of the alkane segment influences the ordering in the SAM. Further elaboration of this observation will be presented in the discussion section. Figure 3b(d) shows the $z$–$V$ spectrum for the T3C8SH molecule.

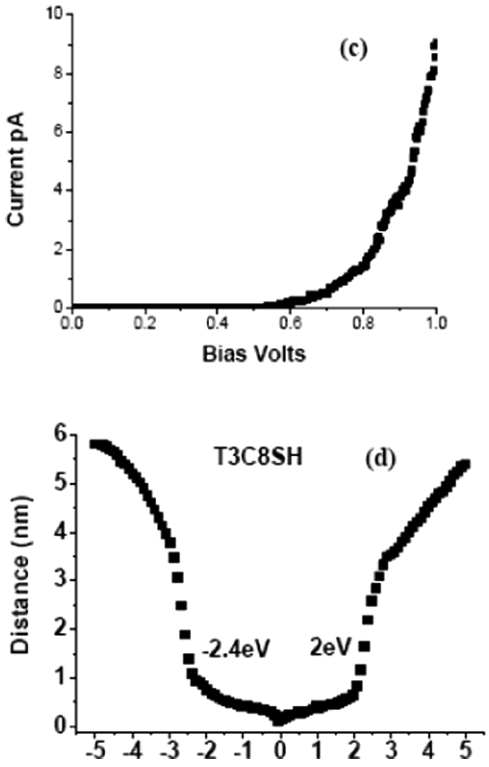


**Figure 3b.** BEEM spectroscopy and $z$–$V$ results for the T3C8SH molecule. (c) BEEM spectroscopy ($I$–$V$). (d) STM $Z$–$V$ spectroscopy showing the HOMO and LUMO levels relative to the Au Fermi level.

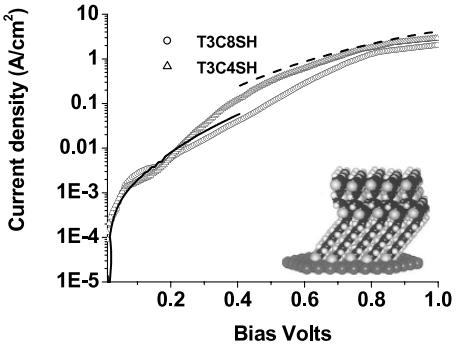


**Figure 4.** $j$–$V$ characteristics of the SAM–Au structures, measured with In counter-electrodes. The solid line is a conventional Richardson–Schottky thermionic emission fit to the data, and is valid for low applied bias. The dashed line is the contribution from tunneling, at high applied bias. See the text for a full discussion.

### 2.2. Discussion

Plots of $j$–$V$ for both the SAMs were obtained by using clean indium counter-electrodes. These are shown in figure 4 on a log scale, with the inset showing the orientation of the molecules on the Au substrate. The molecular layer itself, as observed in an STM shows no voids or inclusions. The packing density of these molecules is expected to be around $3 \times 10^{14}$ cm$^{-2}$ with an area of almost 25 A$^2$ per molecule [40]. The contact area, as determined by the In counter-electrode's physical boundaries, for both samples was 0.25 mm$^2$. The total current shows a complex dependence on voltage over the voltage sweep range of 0–1 V. As expected, the current through the longer T3C8SH molecule is smaller than the current through the T3C4SH molecule. It is also evident that a single function would be unable to fit the $j$–$V$ curves since the molecules have two segments, and the HOMO is predominantly on one. Therefore, we analyze these $j$–$V$ curves following the treatment of Salomon *et al* [41]. Figure 4 also shows two fits, the solid line indicating charge injection across a Schottky barrier, and the dashed line indicating

tunneling. The Schottky fit is as per the standard relation:

$$j = K \exp(-q(n\phi_b - V)/nkT) \quad (1)$$

where $K$ is a constant, $q$ is the electron charge, and $k$ is Boltzmann's constant. From the slope of the $\ln(j)$–$V$ curve, we find that the ideality factor, $n$, ranges from 2.4 to 7. The $\phi_b$ can be determined from the intercept of this plot to be 0.54. As the effective barrier ($n\phi_b$–$V$) decreases with increasing $V$, the effect of the Schottky barrier decreases, and tunneling through the organic molecular layer becomes the limiting factor for transport.

The dashed line which indicates tunneling is of the form

$$j = j_0 e^{-\beta d} \quad (2)$$

where $d$ is the thickness of the organic molecular layer, 1.2 nm for T3C4SH and 1.6 nm for T3C8SH as measured by x-ray reflectometry (not shown) on Ag/SAM/Au trilayers, which show diode behavior. It should be borne in mind that the use of dissimilar metals causes larger error bars in this measurement. $\beta$ is the inverse tunneling decay length, and is given by the following relation:

$$\beta = 4\pi\sqrt{((2m^*(\phi_t - qV/2))/h^2)^-} \quad (3)$$

for a rectangular tunneling barrier. $m^*$ is the effective mass, and $h$ is Planck's constant. To extract absolute values for $\phi_t$ and $m^*$, an independent measurement of one of these quantities is required. Joachim and Magoga [42] have calculated the effective mass $m^*$ and $\beta$ for electrons while tunneling through several molecular wires. Using their reported values of 0.3 for $\beta$, and $0.16m_0$ for $m^*$ for a similar molecule, a tunneling barrier may be obtained which gives reasonable fits to the experimental data. By this method, we obtain a tunneling barrier of 1.1 eV. This appears reasonable, since the carriers are already in the HOMO segment of the T3, and in principle, merely need to cross over into the HOMO of the short alkane segment. Zhitenev *et al* [43] have discussed possible transport mechanisms, through SAMs. Given the values of the Schottky barrier, the tunneling barrier, and knowing the work functions of Au and Ag, it now becomes possible to determine the bond dipole at the Au–SAM interface, arising from the Au–S bond. The strength of this dipole turns out to be −1.3 eV, using work functions of 4.5 for Ag, and 5.1 for Au respectively. This result is in agreement with the results of Heimel *et al* [44] whose theoretical studies of the interface energetics at metal–molecule junctions, specifically thiols on Au, yielded a bond dipole for the Au–S bond of −1.19 eV.

Figure 5 presents the band alignments for the interfaces between Ag/T3C4SH/Au (a) and Ag/T3C8SH/Au (b). As the SAM molecules comprise two segments, that is, the $\alpha$-functionalized terthiophene (T3) with alkanethiol (C4SH or C8SH) anchoring groups, the highest occupied molecular orbital (HOMO) and lowest unoccupied molecular orbital (LUMO) of individual segments are depicted in the schematic diagrams. In these figures, the charge injection from silver into terthiophene gives a barrier of 0.5 eV as probed using the BEEM technique, which is shown by the dotted ellipse. The

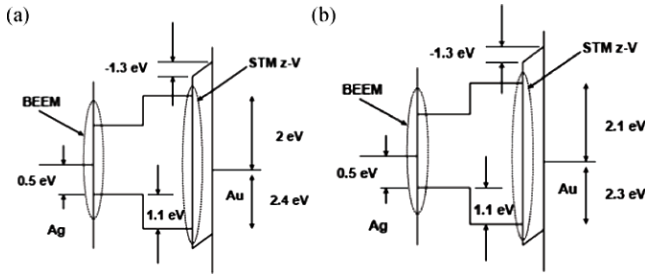


**Figure 5.** Energy level alignment across the Ag–SAM–Au interfaces for (a) T3C8SH and (b) T3C4SH. Please see the text for a detailed discussion.

hole and electron injection barriers of the anchoring molecule with respect to the Fermi level of template-stripped gold as obtained using STM $z$–$V$ technique are each found to be 2.3 and 2.1 eV for the T3C4SH SAM as indicated by the dotted circle. The corresponding numbers for the T3C8SH SAM are 2.4 eV and 2 eV respectively. The STM $z$–$V$ technique has been applied to some organic films a few nanometers thick on gold surfaces [36]. However, in this study the SAMs are bonded directly to Au atoms via the thiol group. Thus a bonding dipole is induced upon SAM formation, as the charge rearrangement upon SAM formation rapidly decays in both the metal and the SAM.

In this experiment, we have two metal films separated by a molecular layer that is approximately 1.5 nm thick. Direct tunneling from one metal electrode to the other is a possibility that needs to be considered. Direct tunneling would make the results of this work open to questions. In order to ensure that the measured collector current is not influenced by tunneling, we carried out a calculation within the framework of the WKB approximation for tunneling from silver through a potential barrier to gold, and compared the simulation with the BEEM results. The parameters were taken based on the assumptions that T3C4SH is a 1 nm long tunneling barrier. The work functions for Ag and Au are taken from published literature. The $I$–$V$ is calculated from the WKB model for a 10 nm$^2$ region. The chosen dimensions for the junction are rough estimates of the spreading area in the metal base caused by ballistic charge carriers due to mutual repulsion. It should be further noted that the tunneling current contribution is $10^{-3}$ pA, or three orders of magnitude smaller than the BEEM current. It should be noted that tunneling does not require the charge carriers to access the molecular electronic energy levels. The only possible explanation for this discrepancy is that our BEEM experiment actually accesses the molecular energy levels, and therefore the collector current is higher than anticipated. A BEEM device is similar to the configuration of a resonant tunneling diode. Resonant tunneling currents are typically much higher than direct tunneling currents [45]. Therefore we can be confident that molecular levels are being accessed.

We now make a few comments on the STM and BEEM images. The Ag film topography indicates grains of 20 to 30 nm average size, with a topography of 1.5 nm over 100 nm scan area, for a nominally 10 nm thick Ag film. The

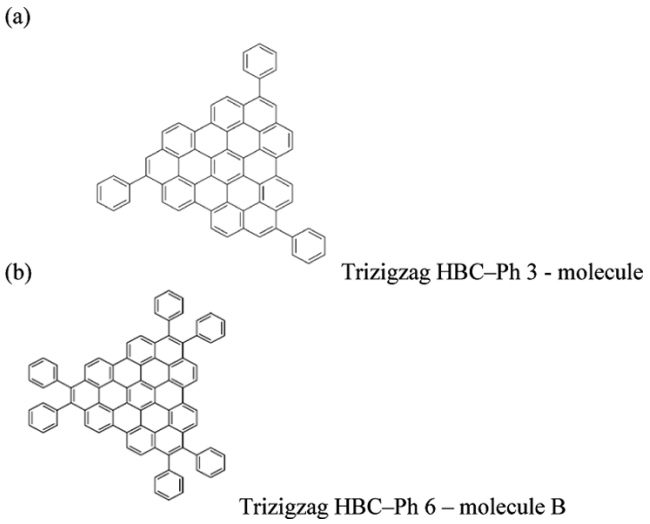


**Figure 6.** Trizigzag-HBC molecules studied in this work. Courtesy of Dr Feng and Professor Muellen, MPI-P. Please see the text for a detailed discussion.

small grain size and flatness are to be expected for Ag films deposited at low temperatures. It should be borne in mind that BEEM current images depend on several factors—topography of the top metal film (base), defects therein, topography of the molecular layer, and its ordering, and topography of the bottom Au layer and defects therein. Clearly, the bright regions in the BEEM images of T3C4SH are caused by low Schottky barrier regions.

Such regions are common for metal–high band gap solids, for example, metal–SiC as well as metal–molecule and metal–organic interfaces. Each of these bright regions may contain several hundreds of molecules. The short alkane segment evidently causes poor ordering in the molecular layer, and the enhanced disorder can create states in the gap, making it easy for injected carriers to access these states and pass through the molecule. On the other hand, for T3C8SH, many bright spots are visible. Although it is tempting to associate each bright spot with a single molecule, such an assignment is open to question, due to the various factors influencing BEEM images, discussed above. However, some topography is still visible above the background of the spots. This clearly does not correspond to the topography of the top Ag film. We believe that these features arise from the topography of the bottom Au film. Much work remains to be done to correlate STM and BEEM images.

## 3. Horizontal molecules

### *3.1. Experimental*

We now present BEEM results for molecules which are flat on the substrate, i.e. horizontal. A typical example would be the hexabenzocoronene (HBC) family of nanographenes. Such molecules have been studied for their potential applications in field effect transistors, light emitting diodes, and also for the construction of bowl shaped sub-units of fullerenes [46].

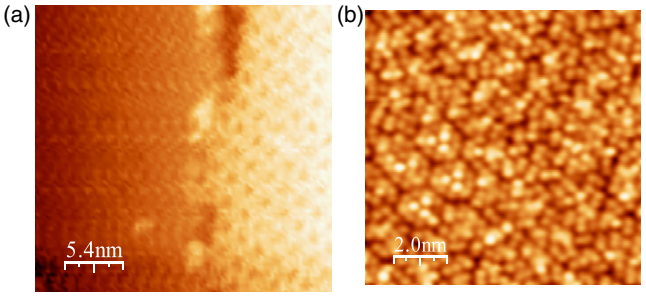


**Figure 7.** STM images of (a) trizigzag-HBC–Ph3, and (b) trizigzag-HBC–Ph6 molecules on the Pt film substrates.

Specifically, we investigate trizigzag-HBC–Ph$x$ ($x = 3, 6$) molecules.

The structure of the molecules is shown in figure 6. The molecules are soluble in trichlorobenzene. Earlier STM studies on these and related molecules at the HOPG–solution interface show ordered domains, with some domain walls present. For physisorbed molecules, molecule–molecule interactions can be stronger than surface–molecule interactions. Except for providing a constraint for planar assembly, the substrate is not a dominating factor in the assembly process. Morgenstern *et al* [47] have shown that iodobenzene can be physisorbed on Cu(111), by deposition of the molecules from solution through a leak valve directly onto the sample which is held at temperatures around 50 K. A similar experimental configuration was adopted for the trizigzag-HBC molecules. The substrates used were e-beam deposited Pt films. Pt has a lattice constant of 3.9 A, and thin films typically expose a (111) surface. Pt does not exhibit surface reconstruction up to high temperatures [48]. However, it can reconstruct in the presence of adatoms at lower temperatures [49, 50]. Therefore, this is a stable substrate, with a spacing of 2.2 A for the (111) planes. This works quite well for the HBC family of molecules investigated in this work, where the molecules are almost equilateral triangles, 2–2.5 nm on a side.

Pt films, nominally 25 nm thick were deposited on glass substrates, using a mechanical mask, so as to aid in the electrical connection for the collector electrode. These served as substrates for the trizigzag-HBC molecules. Subsequently, the Pt films were exposed to a vapor of the molecules dissolved in trichlorobenzene, through a precision leak valve, onto the substrates held at liquid nitrogen temperatures. This resulted in a few layers of the target molecule on the Pt substrate, after the pressure near the substrate vicinity was maintained in the high $10^{-7}$–$10^{-6}$ Torr range for several tens of seconds. Unfortunately, there is no *in situ* diagnostic tool available in the chamber to determine the number of layers of molecules deposited. After this, the substrate was warmed to 100 K in order to desorb any entrapped solvent molecules. STM $z$–$V$ spectroscopy and BEEM were done on these films, in the same system as was used for the previous set of molecules. BEEM experiments involved further deposition of a nominally 7–8 nm thick Pt film on top of the molecular layer. The experimental results are discussed below.

Figures 7(a) and (b) show STM images of these molecules on the Pt film substrates. Figures 8(a) and (b) show the STM

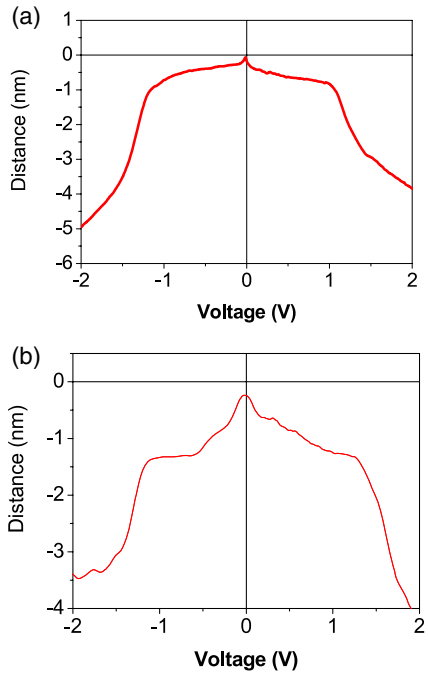


**Figure 8.** STM $z$–$V$ spectroscopy of (a) trizigzag-HBC–Ph3, and (b) trizigzag-HBC–Ph6 molecules on Pt substrates.

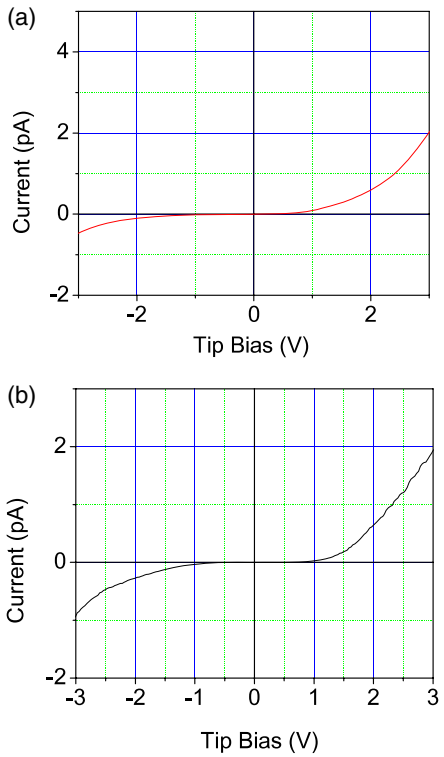


**Figure 9.** BEEM spectroscopy of (a) trizigzag-HBC–Ph3, and (b) trizigzag-HBC–Ph6 molecules on Pt substrates.

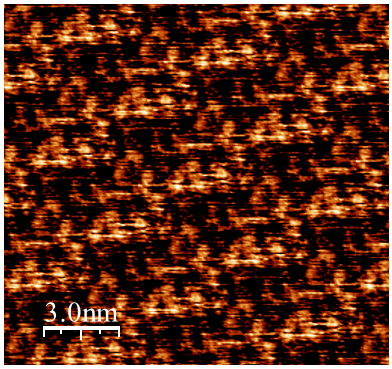


**Figure 10.** Molecular scale resolution BEEM current image for trizigzag-HBC–Ph6 molecules on Pt substrates.

$z$–$V$ spectroscopy results on molecules A and B respectively. As usual, the points of inflection in the STM $z$–$V$ correspond to the electron and hole polaron binding energies, or the LUMO and HOMO respectively. The corresponding packing geometries are as indicated in the insets to these images. Therefore, with respect to the Fermi level of the Pt substrate, for molecule A, the HOMO lies 1.1 eV below, and the LUMO is 1.2 eV above it. This yields a HOMO–LUMO gap of 2.3 eV, which corresponds quite well to electrochemical measurements [59]. For molecule 2, the HOMO is 1.2 eV below the Fermi level of the Pt substrate, while the LUMO is 1.2 eV above the Fermi level of Pt. This corresponds to a HOMO–LUMO gap of 2.4 eV. Again, this corresponds reasonably well to electrochemical measurements of the HOMO–LUMO gap.

Figures 9(a) and (b) show the BEEM spectroscopy results for molecules A and B respectively. These molecules exhibit ambipolar transport, and should be contrasted with the thiophene molecules discussed in the previous section, which transport only holes. As usual, the points of departure of the $I$–$V$ from the $x$-axis would correspond to the electron and hole injection energies, or the LUMO and HOMO respectively. Therefore, with respect to the Fermi level of the Pt base, for molecule A, the HOMO lies 0.8 eV below, and the LUMO is 1 eV above it. This yields a HOMO–LUMO gap of 1.8 eV, which should be compared and contrasted with the STM $z$–$V$ spectroscopy results presented above. For molecule 2, the HOMO is 0.9 eV below the Fermi level of Pt, while the LUMO is 0.9 eV above the Fermi level of Pt. This yields a HOMO–LUMO gap of 1.8 eV, which should be compared and contrasted with the STM $z$–$V$ spectroscopy results presented above. The reasons for this discrepancy between the STM $z$–$V$ and BEEM spectroscopy results can be attributed to states induced in the HOMO–LUMO gap of the molecule. This will be discussed in the next section below.

For these horizontal molecules, BEEM current images show more uniform transport across the molecule. A representative image is shown in figure 10. Molecule scale resolution can be discerned, at least for the trizigzag-HBC–Ph6 molecule. Work is still in progress with these molecules, and more comprehensive results will be presented elsewhere.

### *3.2. Discussion*

Xue and Ratner [22, 23] have studied the transmission across an Au–phenyl dithiol (PDT) and an Au–bi-phenyl dithiol (BPD) structure. Most of the potential drop occurs at the

Au–phenyl ring interface. Once charge is transferred from Au to the phenyl ring, further transport does not change the potential, although it is accompanied by changes in the electron density on the molecules. In the case of the interfaces studied here, one can assume that the primary injection process is the transfer of charge from the metal to the molecular layer in the immediate vicinity of the metal.

Therefore, using a three-step model for BEEM [9, 10], it is possible to determine the transmission function for the metal–molecule interface [51]. Comparing the normalized transmission function determined from experimental data with the calculation of Xue and Ratner [22, 23] yields two common features: (a) both have a curvature that is concave upwards, i.e. they scale with a power of energy, which is greater than one, (b) both peak towards the HOMO levels of the organic. Given the crude approximations that have been made, the agreement between theory and experiment is noteworthy. In contrast, for a MIS interface, the transmission function is the available density of states in the semiconductor, and scales with $E^{1/2}$.

Metal induced gap states or metal wavefunctions tailing into the gap of inorganic semiconductors are well established [52, 53]. Recently, there has been an appreciation of the importance of such states in MO contacts. Theoretical calculations [22, 23] have shown that MIGS can arise from proximity of metal to the organic. Experimental verification of MIGS in PPV has been published recently [54]. An electrochemically gated transistor was used to probe the density of states (DOS). The important findings in this work are: significant tailing of the metal DOS into the gap, the assignment of the HOMO (determined by cyclic voltammetry) in the literature is not exact, and the tail of the DOS in the gap has quite a complex structure.

The geometry of a BEEM device is such that it can also be analyzed as a resonant diode. It is therefore appropriate to use the relation for a resonant diode to determine the LDOS (local density of states) from the transmission function. The relation is

$$I = (2e/h)S\mu \tag{4}$$

where $S$ is the LDOS, $I$ the current, and $\mu$ the energy. The LDOS, which can be determined from the transmission function for different metal–molecule interfaces, is shown in figure 11. The important point to note is that the LDOS depends on the ratio of the atomic core potentials of the metal and organic [52]. For organics, one may take the atomic core potential to be that of carbon. For noble metals such as those used in this work, the atomic core potential may be obtained from the literature. Consistently with the observations of Muelenkamp *et al* [54], we observe significant tailing of electronic states into the gap, particularly in the vicinity of the molecule HOMO. In addition, we also find that the HOMO as determined from the LDOS does not peak at the transmission. This appears to be a consequence of the proximity of the HOMO of most molecules to the Fermi level of the high work function metals used in this work.

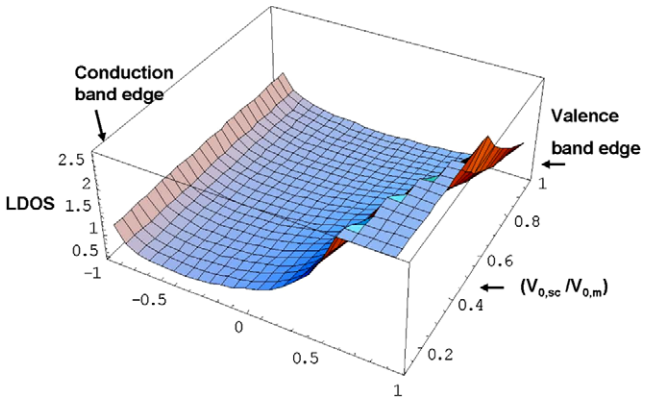


**Figure 11.** Plot of the density of states in the gap, as a function of the energy in the band gap, and the ratio of potentials of semiconductor and metal ($V_{0,\mathrm{sc}}/V_{0,\mathrm{m}}$). The edge of the conduction band is to the left of the figure, and the edge of the valence band to the right.

## 4. Concluding remarks

We have successfully applied the BEEM technique to study charge transport across metal–organic and metal–molecule interfaces with nanometer scale spatial resolution. Inhomogeneous charge injection has been observed for metal–upright molecule interfaces. For the horizontal molecules, the BEEM current images show uniform charge injection across the interface, and molecule scale resolution is visible. Whether this arises due to the focusing effect of the electrons due to the top metal electrode remains to be investigated [9, 10]. BEEM in conjunction with STM $z$–$V$ spectroscopy is a powerful technique for studying metal–molecule interfaces with nanometer scale resolution. It is possible to determine the entire band alignment across the metal–molecule–metal structure by combining these two techniques.

Inhomogeneous charge injection however does not preclude device applications, since Schottky barrier inhomogeneities are also seen with inorganic semiconductors such as silicon carbide [55]. Recent work with self-assembled monolayers of molecules which exhibit negative differential resistance (NDR) has been controversial [56]. It is now acknowledged that the observed NDR may not be due to the electrical characteristics of the molecules, but could arise due to the creation and destruction of conducting metallic filaments. We have shown in earlier work that such filaments arise naturally at low Schottky barrier patches [57]. Similar results have been reported for other systems [58].

Roughness, microstructure of the metal, topography of the organic and microstructure of the organic film are all factors which influence the BEEM current image. The connection between local defects/microstructure and electronic properties is by now generally acknowledged [22, 23]. Therefore, controlling microstructure of the metal and ordering the molecular layer can increase the uniformity of charge injection and improve the performance of devices.

## Acknowledgments

The molecules used in this work were provided by Professors P Baeuerle, K Muellen, and Dr Xinliang Feng. Discussions with Professors W Knoll, K Muellen, P Baeuerle, and Dr Xingliang Feng are gratefully acknowledged. Part of this work was supported by IMRE, an A*Star Research Institute, Singapore.

## References


[1] Aviram A and Ratner M 1974 *Chem. Phys. Lett.* **29** 277
[2] Green J E, Choi J W, Boukai A, Bunimovich Y, Johnston-Halperin E, DeIonno E, Luo Y, Sheriff B A, Xu K, Shin Y S, Tseng H R, Stoddart J F and Heath J R 2007 *Nature* **445** 414
[3] Ishii H, Sugiyama K, Ito E and Seki K 1999 *Adv. Mater.* **11** 605
[4] Gittins D I, Bethell D, Schiffrin D J and Nichols R J 2000 *Nature* **408** 67
[5] Donhauser Z J, Mantooth B A, Kelly K F, Bumm L A, Monnell J D, Stapleton J J, Price D W, Rawlett A M, Allara D L, Tour J M and Weiss P S 2001 *Science* **292** 2303
[6] Lau C N, Stewart D R, Williams R S and Bockrath M 2004 *Nano Lett.* **4** 569
[7] Sakamoto T, Sunamura H, Kawaura H and Hasegawa T 2003 *Appl. Phys. Lett.* **82** 3032
[8] De Boer B, Frank M M, Chabal Y J, Jiang W, Garfunkel E and Bao Z 2004 *Langmuir* **20** 1539
[9] Narayanamurti V and Kozhevnikov M 2001 *Phys. Rep.* **349** 447
[10] Prietsch M 1999 *Phys. Rep.* **253** 163
[11] Garcias D H, Tein J, Breen T L, Hsu C and Whitesides G M 2000 *Science* **289** 1170
[12] Metzger R M, Xu T and Peterson I R 2001 *J. Phys. Chem.* B **105** 7280
[13] Zhou C, Deshpande M R, Reed M A, Jones L and Tour J M 1997 *Appl. Phys. Lett.* **71** 611
[14] Cui X D *et al* 2001 *Science* **294** 571
[15] Wang W, Lee T and Reed M A 2003 *Phys. Rev.* B **68** 035416
[16] Nazin G V, Qiu X H and Ho W 2003 *Science* **302** 77
[17] Zhitenev N B, Erbe A, Bao Z, Jiang W and Garfunkel E 2005 *Nanotechnology* **16** 495
[18] Datta S *et al* 1997 *Phys. Rev. Lett.* **79** 2530
[19] Boulas C *et al* 1996 *Phys. Rev. Lett.* **76** 4797
[20] Kornilovitch P E, Bratkovsky A M and Stanley W R 2002 *Phys. Rev.* B **66** 165436
[21] Temirov R, Soubatch S, Lucian A and Tautz F S 2006 *Nature* **444** 350
[22] Xue Y and Ratner M 2003 *Phys. Rev.* B **68** 115406
[23] Xue Y and Ratner M 2003 *Phys. Rev.* B **70** 081404
[24] Li W J, Kavanagh K L, Matzke C M, Talin A A, Leonard F, Faleev S and Hsu J W P 2005 *J. Phys. Chem.* B **109** 6252
[25] Ozcan S, Smoliner J, Andrews M, Strasser G, Dienel T, Franke R and Fritz T 2007 *Appl. Phys. Lett.* **90** 92107
Haick H *et al* 2006 *Phys. Status Solidi* a **203** 3438
[26] Bannani A, Bobisch C and Moeller R 2007 *Science* **315** 1824
[27] Kirczenow B 2007 *Phys. Rev.* B **75** 045428
[28] Wagner P, Hegner M, Guntherodt H J and Semenza G 1995 *Langmuir* **11** 3867
[29] Frisch M J *et al* 2004 *Gaussian 03, Revision C.02* (Wallingford, CT: Gaussian)
[30] Suhai S 1995 *Phys. Rev.* B **51** 6553
[31] Millefiori S, Alparone A and Millefiori A J 2000 *J. Heterocyclic Chem.* **37** 847
[32] Champagne B, Mosley D H and Andre J M 1994 *J. Chem. Phys.* **100** 2034
[33] Zhou A, Ren A M and Feng J K 2004 *Polymer* **45** 7747
[34] Colditz R, Grebner D, Helbig M and Rentsch S 1995 *Chem. Phys.* **201** 309
[35] Beljonne D, Shuai Z and Bredas J L 1993 *J. Chem. Phys.* **98** 8819
[36] Alvarado S F, Seidler P F, Lidzey D G and Bradley D D C 1998 *Phys. Rev. Lett.* **78** 1082
[37] Bell L D and Kaiser W J 1996 *Annu. Rev. Mater. Sci.* **26** 189
[38] Ludeke R and Prietsch M 1991 *J. Vac. Sci. Technol.* A **9** 885
[39] Baeuerle P 2007 private communication
[40] Liedberg B, Yang Z, Engquist I, Werde M, Gelins U, Gotz G and Baeuerle P 1997 *J. Phys. Chem.* B **101** 5951
[41] Salomon A, Boecking T, Chan C K, Amy F, Girshevitz O, Cahen D and Kahn A 2005 *Phys. Rev. Lett.* **95** 266807
[42] Joachim C and Magoga M 2002 *Chem. Phys.* **281** 347
[43] Zhitenev N B, Erbe A and Bao Z 2004 *Phys. Rev. Lett.* **92** 186805
[44] Heimel G, Romaner L, Bredas J L and Zojer E 2006 *Phys. Rev. Lett.* **96** 196806
[45] Datta S 2005 *Quantum Transport—from Atom to Transistor* (Cambridge: Cambridge University Press)
[46] Feng X, Wu J, Ai M, Pisula W, Zhi L, Rabe J P and Muellen K 2007 *Angew. Chem. Int. Edn* **46** 3033
[47] Jaeckel F, Watson M D, Muellen K and Rabe J P 2006 *Phys. Rev.* B **73** 045423
[48] Morgenstern K, Hla S W and Rieder K–H 2003 *Surf. Sci.* **523** 141
[49] Bott M, Hohage M, Michely T and Comsa G 1993 *Phys. Rev. Lett.* **70** 1489
[50] Sandy A R, Mochrie S G J, Zehner D M, Gruebel G, Huang K G and Gibbs D 1992 *Phys. Rev. Lett.* **68** 2192
[51] Troadec C, Jie D, Kunardi L, O'Shea S J and Chandrasekhar N 2004 *Nanotechnology* **15** 1818
[52] Heine V 1965 *Phys. Rev.* A **138** 1689
[53] Monch W 2004 *Electronic Properties of Semiconductor Interfaces* (Berlin: Springer)
[54] Hulea I N, Brom H B, Houtepen A J, Vanmaekelbergh A, Kelly J J and Meulenkamp E A 2004 *Phys. Rev. Lett.* **93** 166601
[55] Im H-J, Ding Y, Pelz J P and Choyke W J 2001 *Phys. Rev.* B **64** 075309
[56] Service R F 2003 *Science* **302** 556
[57] Kunardi L, Troadec C and Chandrasekhar N 2005 *J. Chem. Phys.* **122** 204702
[58] Terabe K, Nakayama T, Hasegawa T and Aono M 2002 *J. Appl. Phys.* **91** 10110
[59] Feng X 2007 private communication